Scientia Iranica B (2022) 29(4), 1767–1781

Sharif University of Technology
Scientia Iranica
Transactions B: Mechanical Engineering
http://scientiairanica.sharif.edu

Investigation of non-Newtonian nano-fluid flow based on the first and second laws of thermodynamics by micro-annulus

F. Mehran[a,*], A. Jabbarzadeh Ghandilou[b], and L.M. Yapanto[c]

a. *Islamic Azad University, Jolfa, International branch, Jolfa, P.O. Box 54417-33574, Iran.*
b. *Department of Mechanical Engineering, University of Tabriz, Tabriz, Iran.*
c. *Faculty of Fisheries and Marine Science, State University of Gorontalo, Jalan Jenderal Sudirman, No. 6 Gorontalo, Indonesia.*

Received 5 July 2020; received in revised form 18 October 2021; accepted 3 January 2022

KEYWORDS
Nano-fluid;
Slip velocity;
Temperature jump;
Finite volume method;
Heat transfer.

Abstract. The current study conducts analyses of the first and second laws for non-Newtonian nano-fluid flow through an annular cylinder filled with non-Newtonian water-CMC/TiO_2 nano-fluid, considering temperature jump and slip velocity. A single-phase pattern was developed for heat transfer and nano-fluid flow. To this end, the impacts of Reynolds number, volume fraction of nano-particles, temperature jump, and slip velocity on the Nusselt numbers and entropy generation were evaluated and the findings on the non-Newtonian performance of the working fluid were reported. According to our findings, due to the higher shear rate in the presence of the interior wall, the Nusselt number of the interior wall was higher than that of the outside walls. Based on the shear-thinning fluid behavior, in case the flow has a higher shear rate, its apparent viscosity would be small. Therefore, it can be concluded that the apparent viscosity of the flow close to the inner wall is low, which reduces the impact of viscosity force and improves heat transfer due to convection-advection phenomenon. In addition, the findings illustrate that the entropy generation ratio is very high at the entrance and decreases along the annular tube. Furthermore, the apparent viscosity of fluid increases by nano-particle volume fraction.

1. Introduction

One of the main obstacles to increasing thermal conductivity in fluids like water is their poor heat transfer properties. Increasing thermal conductivity has a significant impact on heat transfer and conduction processes. Solids containing high thermal conductivity cause the suspension formation of fine metal solid particles called nanofluids, i.e., a mixture of nanoparticles in a base fluid that improves its heat transfer. Different types of particles such as metallic, non-metallic, and polymeric can be added to the base fluid. Particles in micrometer and millimeter dimensions can cause many problems such as sedimentation, corrosion, and pressure drop [1]. On the contrary, nano-sized particles ensure higher stability and significantly increase the thermal conductivity. In addition, they cause less pressure drop than particles in micrometer and millimeter dimensions [2]. Two main factors that affect Entropy Generation (EG) include heat transfer and viscosity effects [3]. In [4] analyzed different effective aspects of EG in thermal engineering. In this respect, the second-law analysis was applied to the EG problem to find an effective way to minimize the irreversibility in empirical engineering and transport procedures.

A considerable problem concerning heat exchang-

*. *Corresponding author.*
E-mail addresses: ghaidaabdulsahib@gmail.com, Farshidmehran@iauj.ac.ir (F. Mehran)

doi: 10.24200/sci.2022.56349.4678

ers and micro-annulus is how to boost the heat transfer performance regardless of pressure drop. In this respect, nano-fluids are considered suitable candidates for this purpose owing to their exceptional feature [5–7], compared to liquids with micro-sized particles [8] which have been already applied in different industries [9–14]. Abdulrazzaq et al. [15] conducted an empirical research on the turbulent heat transfer through a nanofluid flow interaction in a cylinder geometry with sharp changes in the flow. Tayebi et al. [16] investigated the natural convective flow process in a magnetic field over the centralized circle path covered by a CNT-water-based nano-liquid.

He et al. [17] presented single- and two-phase patterns for heat transfer and flow analysis in the case of CuO-water nanofluid. They suggested that the application of one twisted tape was found more effective. The length effect in macro- and micro-scale problems was different [18], indicating the necessity of considering this difference in heat and mass transfer systems in researches. In this regard, slip velocity and temperature jump are two consequential issues that should be taken into account.

Fu et al. [19] evaluated the impacts of nanoparticles as well as the slip and temperature jump in non-Newtonian nano-fluids. To determine whether or not velocity slip and temperature jump should be considered in a certain channel size, a dimensionless parameter called Knudsen number (Kn) should be used [20] based on which some researchers have examined the heat transfer and flow of micro-scale systems [21–24]. For instance, Malvandi and Ganji [25] studied the slip velocity for alumina/water nano-fluid in a circular microchannel within a fix magnetic field. Zhang et al. [26] analytically analyzed heat distribution in a two-dimensional micro-scale channel considering the same boundary conditions. They considered walls to be adiabatic under fixed heat rate boundary conditions. Talavari et al. [23] conducted a study on the rarefaction of heat transfer of a micro-tube flow, considering the slip velocity conditions. They found that Nu number decreased upon increasing the Kn number. In addition, the non-dimensional parameters Kn affected the temperature field in the flow under slip-flow conditions. Kn indicates the rarefaction impact. Shamshiri et al. [27] conducted the first and second law analyses of a rarefied gas in a rotating annulus. They investigated the slip and jump conditions affecting the interior and exterior walls in velocity and temperature fields. Pathare et al. [21] analytically and numerically examined the pressure-driven nitrogen slip flows in a long rectangular micro-channel by determining the temperature of a steady state wall under boundary conditions. Reddy et al. [22] investigated the impacts of changes in the exterior forces on the fluid in rough nano-scale channels with different inner wall structures.

In [28], EG was investigated in a micro-annulus. The laminar flow at the walls was considered at the constant heat rate and first-order slip velocity. The findings demonstrated that EG decreased upon increasing Kn. Zhao [29] analyzed heat distribution and EG considering the forced convection in a micro-electro-mechanical procedure in the slip-flow. Erbay et al. [30] reported that the value of EG was high at the entrance and then, it decreased dramatically. Of note, EG value was almost negligible at the centerline while it reached its maximum value in close proximity to the walls of the parallel plate microchannels.

Karimipour et al. [31] studied the impact of temperature and mass fraction of CuO nano-particles on the nano-fluid analysis. They concluded that the Pr number was more relative to the mass fraction of nanoparticles than the temperature. Jangili et al. [32] evaluated the EG of micro-polar fluid in a vertical cylinder where both inner and outer walls were rotating. They found that the EG was in close proximity to the interior rotating cylinder surface since the high temperature and velocity rates were maximum.

Recently, the application of non-Newtonian fluids has considerably increased owing to the widespread utilization of non-Newtonian fluids, especially on a micro scale [33–35]. Most fluids in chemical engineering, bio-engineering, and industries can be considered as non-Newtonian fluids. Abdulrazzaq et al. [36] studied heat transfer and EG of different types of fluids flowing through parallel-plates. For this purpose, they considered the slip velocity and viscous dissipation effect of the bot wall and found that upon increasing the slip coefficient, Nu number and Bejan number increased and the EG rate decreased. In another study [37], they investigated the heat transfer of the power-law slip and plug flows. Both parallel-plate and circular microchannel with slip walls were considered in the mentioned study. They employed the perturbation approach to analytically solve the governing equations and carried out numerical simulations to verify their results. Anand [38] analytically measured the heat transfer rate of a power-law fluid in a micro-scale channel. They considered three different laws in modeling the slip wall conditions. According to their findings, the values of Nu and EG ratios were higher and lower, respectively, than the corresponding values for other slip laws. More recently, Kiyasatfar [39] and Ramanuja et al. [40] conducted another study on heat transfer and EG non-Newtonian fluid. The non-linear slip and viscous dissipation were considered to solve equations analytically. They reported that the heat transfer and EG rates were significantly affected by slip and viscous dissipation, especially in the case of dilatant fluids. They also found that the Nu number increased by increasing the slip coefficient, while the EG rate followed an inverse trend. In addition, the velocity

pattern decreased by increasing the slip parameter. Li et al. [41] evaluated the rheological performance of MgO-water in different volume fraction ranges of nanofluid under different conditions. Their results confirmed a decrease and then, an increase in the viscosity at high temperatures in the presence of more solid volume fraction of nanoparticles.

As discussed in previous studies, nano-fluids play a key role in heat transfer; therefore, investigation of the involved parameters significantly improves the heat transfer. Given that the movement of non-Newtonian nano-fluid flow through the annular cylinder is one of the most practical physics in industries, the current study evaluated the impact of slip velocity and temperature jump condition for this geometry. In this regard, both heat transfer and EG of the non-Newtonian nano-fluid flow in micro annulus were numerically investigated. In addition, the viscosity change and shear rates as well as the thickness and velocity boundary layer development in the non-Newtonian nano-fluid flow were measured through the volume fraction method. Consideration of the boundary condition in flows with micro-scale geometries is of significance. Although a number of studies have been conducted on this subject, there has always been a gap for different geometries. In this respect, the present study was conducted considering different volume fractions of Nano-particles, Reynolds number, and slip velocity. The impacts of the temperature jump, slip velocity, and volume fraction of nanoparticles on the heat transfer ratio and EG were evaluated, considering the viscous effect and heat transfer.

2. Methodology

The current study considered a micro-annulus characterized by an inlet and an outlet. To reduce the time of numerical simulation, the axisymmetric assumption was taken into account given the geometry symmetry in terms of the axis and the flow in two-dimensional geometry was modeled. Figure 1 depicts the physical model and coordinate system. The length of geometry (L) was 10 mm, and the radii of the inner and outer cylinder were 0.2 and 0.4 mm, respectively. In the cold non-Newtonian nano-fluid water-CMC/TiO_2, streams were imposed on the hot wall at $T_W = 35°C$.

Under initial conditions, the flow and heat transfer fields were regarded as the axial symmetries, and Finite Volume Method (FVM) was developed to analyze the equations. The upwind scheme was also used to analyze the displacement expressions in the survival equations. It is assumed that at two inputs, the current enters at a uniform temperature and velocity, whose networking is shown in Figure 2.

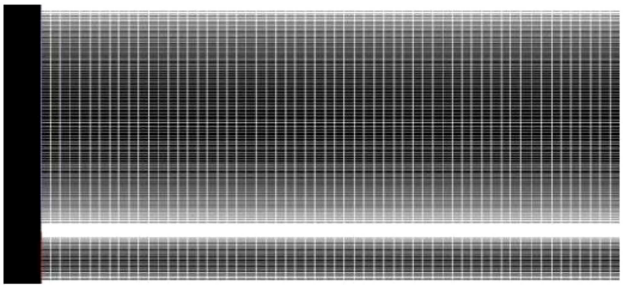

Figure 2. Sample of the generated network.

2.1. Government equations

The heat transfer ratio and EG of the single-phase non-Newtonian nano-fluid flow in the micro-annulus were investigated in this study. The flow was found to be steady-state, laminar, and axisymmetric. Given the very small size of the particles, it was assumed that nanoparticles and basic fluid were in thermal balance at a constant velocity; hence, a single-phase assumption was sufficient. Equations for the mentioned flow include continuum, momentum, and energy, as given below [42]:

$$\nabla.\vec{U} = 0; \quad \frac{\partial u}{\partial x} + \frac{\partial v}{\partial y} = 0,$$

$$u\frac{\partial u}{\partial x} + v\frac{\partial u}{\partial R} = -\frac{\partial P}{\partial x} + \frac{1}{\mathrm{Re}_{nf}} \left[\frac{\partial}{\partial x}\left(\frac{\partial u}{\partial x}\right)^n + \frac{\partial}{\partial R}\left(\frac{\partial u}{\partial R}\right)\right]^n, \quad (1)$$

$$u\frac{\partial v}{\partial x} + v\frac{\partial v}{\partial R} = -\frac{\partial P}{\partial x} + \frac{1}{\mathrm{Re}_{nf}} \left[\frac{\partial}{\partial x}\left(\frac{\partial v}{\partial x}\right)^n + \frac{1}{R}\frac{\partial}{\partial R}R\left(\frac{\partial v}{\partial R}\right)\right]^n - \frac{v^2}{R}, \quad (2)$$

$$\vec{U}.\vec{\nabla}T = \left(k_{nf}/\rho_{nf}C_{p\,nf}\right)\nabla^2 T,$$

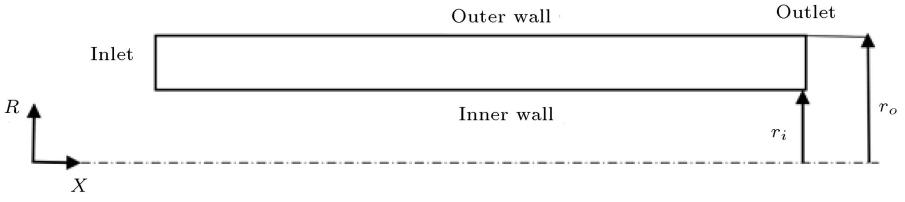

Figure 1. Schematic geometry of the research model.

$$u\frac{\partial T}{\partial x}+v\frac{\partial T}{\partial R}=\frac{1}{\mathrm{Re}_{nf}.\mathrm{Pr}_{nf}}\left[\frac{\partial}{\partial x}\left(\frac{\partial T}{\partial x}\right)^{n}+\frac{1}{R}\frac{\partial}{\partial R}R\left(\frac{\partial T}{\partial R}\right)\right]^{n}, \tag{3}$$

where P is the pressure; $\vec{U}$ presents the velocity value and direction; u and v are the velocity parts along the x and R axes, respectively; T stands for the temperature; ρ_{nf}, k_{nf}, $C_{p_{nf}}$ denote the density, thermal conductivity, and specific heat of the nanofluid, respectively; and n is the number of power-law fluids. The sample $n=1$ is indicative of a Newtonian fluid. Re_{nf} and Pr_{nf} represent the Reynolds and Prandtl numbers of the nanofluid. The shear stress tensor is presented as [43]:

$$\rho_{nf}\vec{U}.\nabla\vec{U}=-\vec{\nabla}P+\nabla.\bar{\bar{\tau}}+\rho\vec{g}+\vec{F};\bar{\bar{\tau}}=\eta\bar{\bar{\dot{\gamma}}}, \tag{4}$$

where $\rho\vec{g}$ is the body force caused by the gravitational acceleration, and $\vec{F}$ and $\bar{\bar{\tau}}$ refer to the external force and stress tensor, respectively. In addition, η is the apparent viscosity and $\bar{\bar{\dot{\gamma}}}$ the shear tensor, expressed below [44]:

$$\bar{\bar{\dot{\gamma}}}=\nabla\vec{U}+\nabla\vec{U}^{T}. \tag{5}$$

The value of η varies depending on fluid type. To be specific, it takes a fixed value in Newtonian fluids; it is correlated to the shear tensor value in non-Newtonian fluid, and it takes a value in power-law non-Newtonian fluid obtained from the following equation [45]:

$$\eta=m\dot{\gamma}^{n-1}, \tag{6}$$

$$\dot{\gamma}=\sqrt{1/2\left(\bar{\bar{\dot{\gamma}}}\bar{\bar{\dot{\gamma}}}\right)}, \tag{7}$$

where $\dot{\gamma}$, η, m, and n stand for the shear rate, apparent viscosity, consistency, and power-law, respectively.

2.1.1. Definition of dimensionless parameters

This study was performed considering different Reynolds numbers obtained from Eq. (8):

$$Re=\frac{\rho_{nf}U_{m}^{2-n}D}{\mu}, \tag{8}$$

where U_m is the mean velocity, D the hydraulic diameter of the annulus, and μ the dynamic viscosity.

Heat transfer could be determined by measuring the Nu for different cases. The Nusselt number is expressed in Eq. (9):

$$Nu=\frac{hD}{k_{nf}}, \tag{9}$$

where h refers to the heat transfer coefficient calculated as:

$$h=\frac{q''}{T_s-T_b}, \tag{10}$$

where T_s, T_b, and q'' denote the surface temperature, fluid bulk temperature, and wall heat flux.

The total EG ratio per unit volume, S_t, can be divided into four portions including heat transfer, viscous dissipation index, mass transfer, and chemical reaction index. In the present study, only the physical aspects of flow were considered; therefore, the chemical reaction and mass transfer terms were eliminated, and two other EG resources namely the heat transfer and viscous dissipation were evaluated [46]:

$$\dot{S}_t'''=\dot{S}_h'''+\dot{S}_f'''. \tag{11}$$

In the present study, there are no coupling phenomenon, mass diffusion, and forces. As a result, EG can be defined by heat transfer as follows:

$$\dot{S}_h'''=\frac{k}{T^2}\left[\left(\frac{\partial T}{\partial x}\right)^2+\left(\frac{\partial T}{\partial y}\right)^2\right], \tag{12}$$

and EG regarding viscosity impact can be expressed by:

$$\dot{S}_f'''=\frac{\eta}{T}\left\{2\left[\left(\frac{\partial u}{\partial x}\right)^2+\left(\frac{\partial v}{\partial y}\right)^2\right]+\left(\frac{\partial u}{\partial y}+\frac{\partial v}{\partial x}\right)^2\right\}. \tag{13}$$

The total EG rate, S_t, EG by viscous impact, S_f, and EG due to the thermal effect, S_h, are then found by integration of their corresponding S''' over the entire volume, V:

$$\dot{S}=\int S'''dV. \tag{14}$$

To determine the thermal and viscous effects on generating entropy, the Bejan number, Be, is used. It is expressed as the irreversibility rate of heat transfer to the whole EG is defined below [47]:

$$Be=\frac{\dot{S}_h}{\dot{S}_t}. \tag{15}$$

2.2. Thermophysical and rheological

This study considered CMC-TiO_2 properties in the simulation of non-Newtonian nano-fluid. In fact, a solution of CMC by 0.45wt% was used as the non-Newtonian base fluid and TiO_2 particles with different volume fractions as nano-particles.

Experimental analysis demonstrated that the thermophysical factors associated with the water-CMC solution for volume fraction less than 6% were similar to water and thermophysical of titanium oxide (TiO_2), as shown in Table 1 [48]. Density and specific heat of non-Newtonian nano-fluid are calculated as follows [49]:

$$\rho_{nf}=(1-\varphi)\rho_f+\varphi\rho_p, \tag{16}$$

Table 1. Thermophysical properties of titanium oxide (TiO_2) particles [23].

Properties	Amount
C_p [J/kgK]	686.2
ρ [kg/m^3]	4250
K [W/mK]	8.9538

$$C_{p_{nf}} = (1-\varphi)\, C_{p_f} + \varphi C_{p_p}, \tag{17}$$

where φ is the volume fraction of nano-particle in the working fluid, and the subscripts nf, f, and p represent the nano-fluid, base fluid, and nano-particle, respectively.

The presented data regarding the conductivity of water-CMC/TiO_2 nano-fluid with different nano-particle concentrations in a previous experimental study [50] were employed for evaluating the thermal conductivity of the working fluid. These values are presented in Table 2.

Table 3 shows the parameters m and n for different volume fractions of nano-particles. The power-law model was utilized to model the non-Newtonian performance of the working fluid. The two rheological parameters in this model include consistency and power-law coefficient. Table 3 lists the values of these parameters for different volume fractions of the TiO_2 nano-particle.

2.3. Boundary conditions

The equations were solved based on uniform temperature and velocity profiles at the inlet, atmospheric pressure at the outlet, and constant temperature at the inner and outer walls of the cylinder. Since some conditions including no-slip and lack of temperature jump boundary conditions might not be suitable for micro-scale flows, the utilized boundary condition can be described as [50]:

Slip velocities are calculated along the walls by:

$$u_s = -\frac{2-F_m}{F_m}\beta\left(\frac{\partial u}{\partial r}\right)_{r=r_o},$$

$$u_s = \frac{2-F_m}{F_m}\beta\left(\frac{\partial u}{\partial r}\right)_{r=r_i}, \tag{18}$$

where β, u_s, and F_m represent the slip velocity, coefficient of the slip velocities, and adaptation, respectively. In addition, the temperature jump values are calculated in the cylindrical geometry as:

$$T_s - T_w = \frac{2-F_t}{F_t}\frac{2\gamma}{\gamma+1}\frac{\beta}{Pr}\left(\frac{\partial T}{\partial r}\right)_{r=r_o},$$

$$T_s - T_w = -\frac{2-F_t}{F_t}\frac{2\gamma}{\gamma+1}\frac{\beta}{Pr}\left(\frac{\partial T}{\partial r}\right)_{r=r_i}, \tag{19}$$

where $\gamma = \frac{C_p}{C_v}$, T_s, T_w, and F_t stand for the special heat, temperature jump (surface), wall temperature, and adaptation of thermal condition, respectively. The present study was carried out under non-slip conditions considering two different $\beta^* = \beta/D$, (0.1 and 0.01). Finally, a comparison was made between the obtained results.

2.4. Numerical methods

The governing equations were solved through the application of the mentioned boundary condition and FVM. A SIMPLE algorithm was used for coupling the velocity with pressure field. A second-order upwind scheme was then selected to discretize energy and momentum. Further, the pressure gradient term was discretized based on a standard scheme. Convergence criteria were set to 10–6 for all variables in all simulated cases.

Table 2. Thermal conductivity of water-CMC/TiO_2 nano-fluid [24].

Percentage of nano-particle volume fraction (φ%)	Thermal conductivity (K [W/mK])
0	0.6
1	0.603
3	0.641
4	0.74

Table 3. Rheological parameters of water-CMC/TiO_2 nano-fluid [25].

Percentage of nano-particle volume fraction (φ%)	Consistency index m[−]	Power-law index n[−]
0	0.145	0.542
1	0.190	0.526
3	0.240	0.502
4	0.365	0.485

3. Grid independency analysis

To prove the independency of the findings of the present study in terms of grid size, four different cell numbers were used to simulate non-Newtonian nano-fluid flow with the volume fraction of 0.04 at a Reynolds number equal to 30. Dimensionless velocity and dimensionless temperature, referred to as the rate of local velocity to uniform velocity at the inlet and the ratio of the local temperature to the difference of inlet and wall temperatures, respectively, were calculated for each case, whose results are given in Table 4. As observed earlier, the mesh with 1000 cells in the axial direction and the mesh with 40 cells in the radial direction are sufficiently accurate.

Table 4. Grid independency for no-slip flow of $\varphi = 0.04$ at $Re = 20$.

Cell number	500-20	750-30	1000-40	1250-50
U	1.3267	1.3318	1.3331	1.3342
θ	0.3207	0.3204	0.3206	0.3206

4. Validation

In order to validate the numerical approach in the present study, the findings of the developed numerical approach were compared with those from [50]. To this end, first, EG in an annulus with non-slip boundary conditions was modeled, and the variation of h_{in} and h_{out} along the annulus length and that of S_f and S_h in the radial direction were calculated. As shown in Figure 2, the result of the present numerical method and the findings obtained in [50] were in good agreement. Then, the heat transfer of non-Newtonian nano-fluid flow in the micro-tube with slip wall and temperature jump was simulated to determine whether or not application of the boundary condition on the walls is valid in the present study. Validation of Nusselt number and dimensionless temperature profile was obtained and compared with the findings of [51]. As shown in Figure 3, the results are in acceptable agreement.

obtained from solving the equations, the addition of the nanoparticles in percentage fraction unit to the heat exchangers decreases the entropy number. As a result, it is practically economical to add these particles as long as the effect of the entropy produced by the pressure drop is negligible. On the contrary, the value of the total heat transfer coefficient increased upon increasing the volume fraction of nanoparticles. To be specific, according to the numerical results, in case the volume fraction of nanoparticles is 6%, the total average heat transfer coefficients, 14%, increase compared to the case where only the base fluid is used. In addition, for a constant amount of heat transfer, application of these nanoparticles reduces the level of heat transfer and, consequently, the volume of the heat exchanger. According to the calculations made for the nanofluid, the nanofluid side pressure increased upon increasing the volume fraction of nanoparticles in a fixed volumetric flow; consequently, addition of 6% nanoparticles to water would result in an increase in the pressure drop of the nanofluid flow up to 80%.

Figure 4 shows the changes in the local EG regarding the heat transfer along different vertical lines in non-Newtonian fluid at different Reynolds numbers. As observed earlier, the magnitude of S_h decreased along the flow direction because the flow at the inlet was not fully developed. In addition, the temperature gradient in the vertical direction was high, hence a high rate of EG. However, the flow becomes fully developed in terms of heat transfer boundary layer in the cross-sections away from the inlet, thus decreasing the temperature gradient dramatically. As a result, the EG rate decreased as well due to the heat transfer.

Figure 4 show the results obtained at different Reynolds numbers. As observed in this figure, increasing the Reynolds number would increase the EG heat

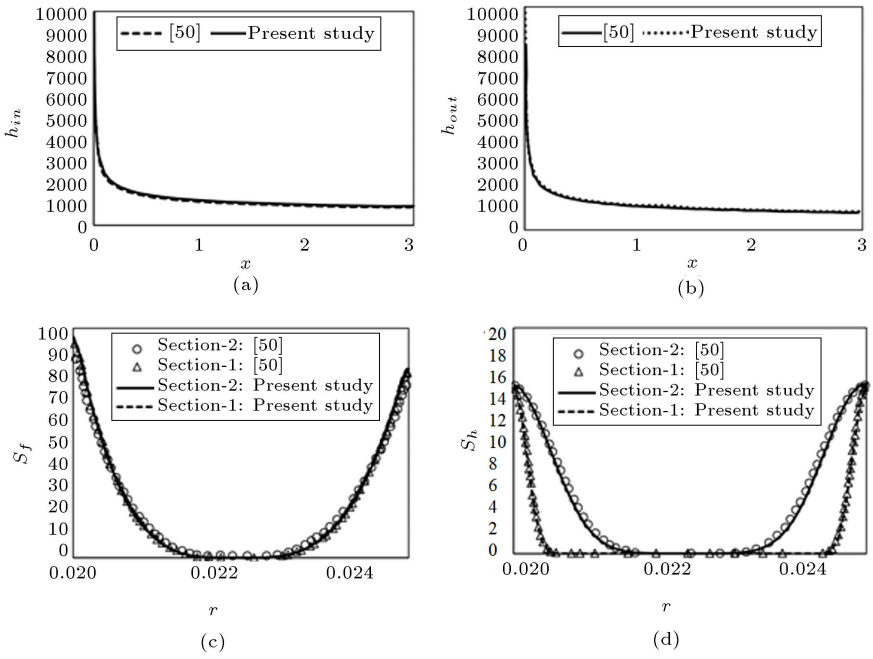

Figure 3. Comparison of the obtained results with [23]: (a) heat transfer on interior walls, (b) heat transfer on outside walls, (c) local friction EG rate at two different cross sections, and (d) thermal EG.

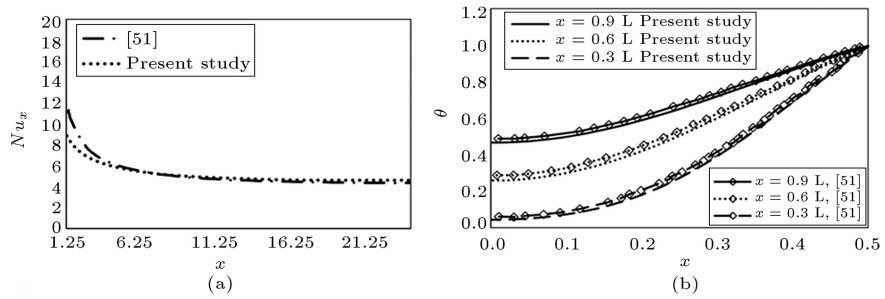

Figure 4. Comparison of the obtained results with [51]: (a) Local Nusselt number and (b) dimensionless temperature profile.

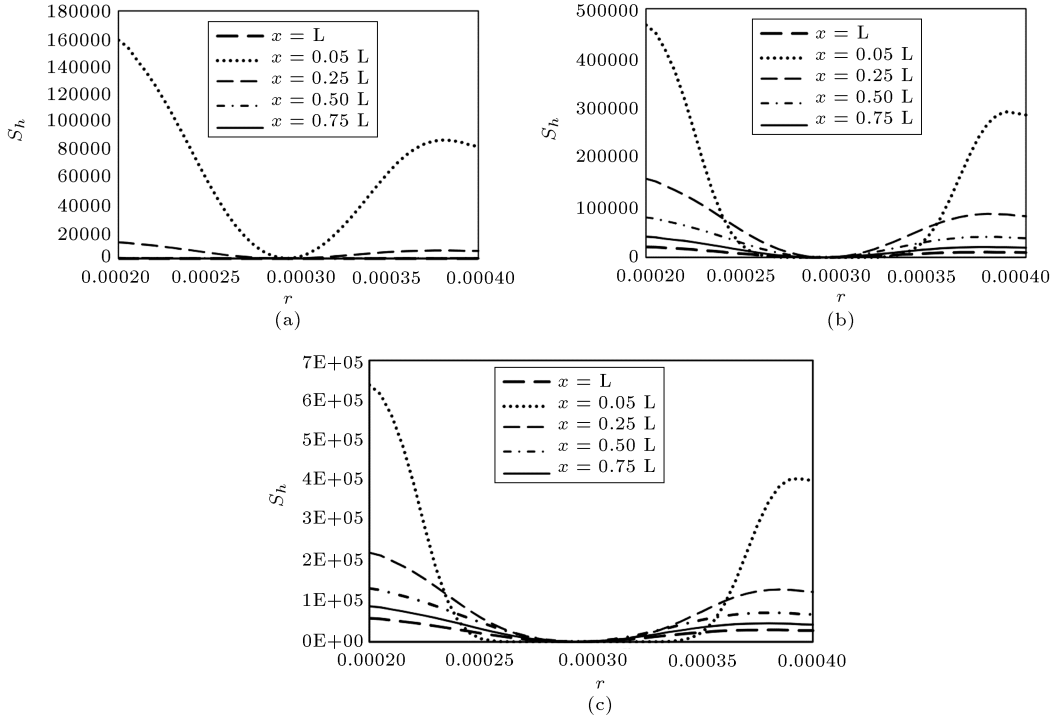

Figure 5. EG rate variation regarding heat transfer for non-Newtonian fluid on different cross-sections at (a) $Re = 1$, (b) $Re = 10$, and (c) $Re = 20$.

transfer rate. In addition, when the Reynolds number of the flow is small, the fluid velocity in the channel becomes small as well, residence time expands, and cool fluid and hot wall will have sufficient time to transfer heat. Consequently, the temperature gradient is lower than large Reynolds numbers.

Figure 5 shows the changes in the Bejan number and EG for different slip coefficients in a non-Newtonian fluid flow with a volume concentration of 4% at a Reynolds number of 10. The EG rate and heat transfer are approximately close to each other under different slip conditions. However, to be specific, the EG rate decreases by increasing the slip wall effect. In addition, at the central line (e.g., $r = 0.0003$), EG rate compared to heat transfer is negligible mainly due to the insignificant temperature gradient in the vertical flow direction.

Figure 5(b) depicts the EG ratio with regard to the viscosity effect in different wall slip conditions. According to this figure, the profile for all slip coefficients is not symmetrical. While the EG value near the central line is negligible, it reaches its maximum value on the walls, especially on the outer wall. In addition, in walls with the no-slip condition, the velocity of fluids in the vicinity of walls is zero; therefore, the fluids experience a high-velocity gradient which results in high EG. When considering the wall under slip condition, the fluid which flows near the wall is characterized by a notable velocity; hence, the velocity gradient is lower than that of the case of no-slip wall condition. Figure 5 proves this theory according to which the EG ratio affected by viscosity effect decreases upon increasing the slip effect.

Figure 6 presents the velocity profiles of u for

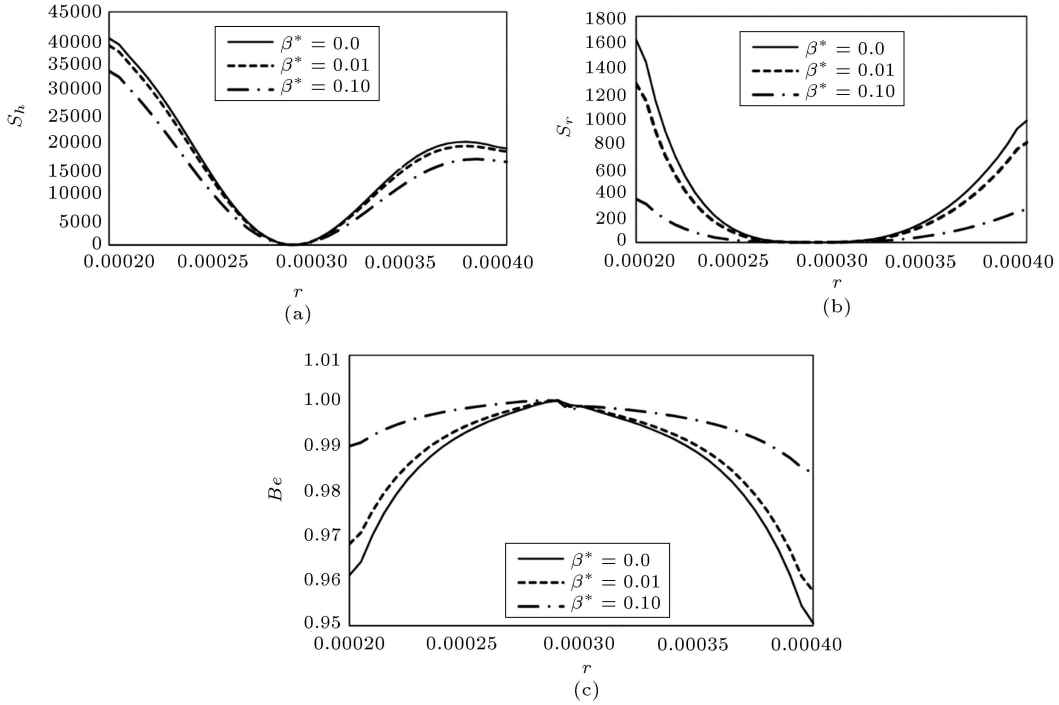

Figure 6. Variation of (a) EG regarding heat transfer, (b) EG regarding the viscous effect, (c) local Bejan number along cross section of $x = L$ for 4 percent volume fraction of nano-particle and $Re = 10$

water-CMC/TiO_2 nano-fluid at $\phi = 0.04$ and laminar Reynolds of 10 for different values of β. Increasing the value of β from 0.0 to $\beta = 0.1$ has a major impact on the velocity profile shapes. Accordingly, the high value of β is attributed to the high velocity at $r = 0.0002$ and $r = 0.0004$ and low $U_{\max}$ at $r = 0.0003$. As observed in Figure 6, the nano-fluid flow is formed in the parabolic function. As a result, different velocity rates can be observed in the walls due to slip boundary conditions.

Figure 7 shows the dimensionless temperature at different Reynolds numbers. According to this figure, the profile of $Re = 1$ is almost linear and close to the unit in all radial locations, while it has a parabolic shape at large Reynolds numbers and its minimum value occurs close to $r = 0.0003$, which decreases upon increasing the Reynolds number. At a small Reynolds number, the flow is of low velocity that results in longer residence time; hence, the fluid temperature reaches the wall temperature. The velocity of fluid flow increases with an increase in the Re; consequently, heat transfer does not occur completely since the fluid temperature is lower than the wall temperature.

Figure 8 presents the dimensionless temperature profile on the vertical lines for different distances from the inlet. As expected, its value on the inner and outer walls for all distances is close to the unit, and the minimum values are obtained close to a radius of 0.0003. This minimum value is zero near the cylinder

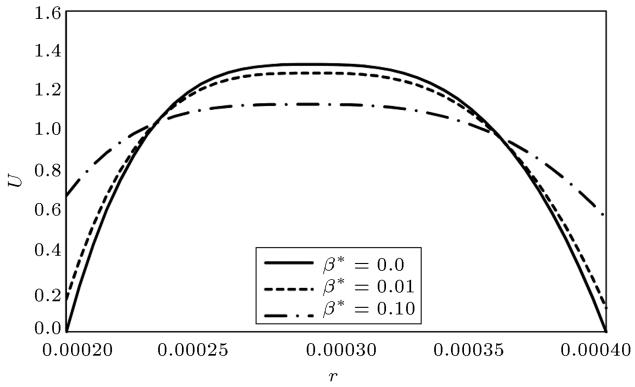

Figure 7. Fully developed velocity profile for non-Newtonian nano-fluid for various slip condition on vertical line $x = 0.75$ L at $Re = 10$

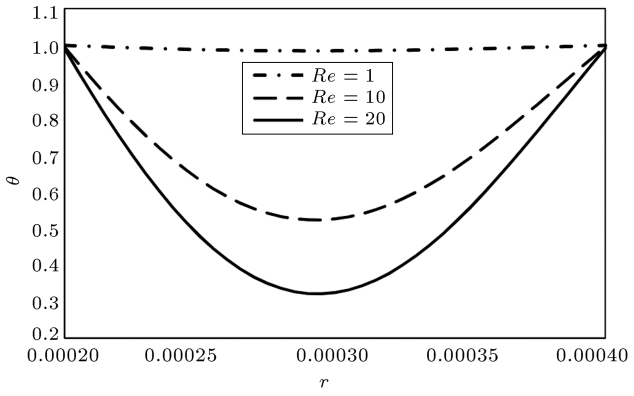

Figure 8. Dimensionless temperature profile for non-Newtonian nano-fluid vertical line at various Re, $\varphi = 0.04$ and $\beta = 0.01$

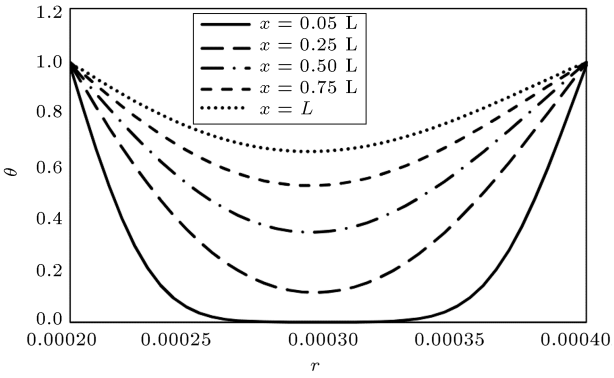

Figure 9. Dimensionless temperature profile for non-Newtonian nano-fluid on various vertical lines, $Re = 10$, $\varphi = 0.04$ and $\beta = 0.01$

entrance ($x = 0.05$ L), while it rises upon increasing the distance from the inlet due to the heat transfer from the hot walls to the cold fluid when fluid flows through the annular cylinder.

Figure 9 shows the dimensionless slip temperature along both inner and outer walls for water-CMC/TiO_2 nano-fluid with $\varphi = 0.04$ at $Re = 10$ under different slip conditions. Slip temperature is affected by slip coefficient; in particular, when $\beta = 0.1$, the effect of fluid temperature is more significant as a result of which the slip temperature is reduced. It also takes a low value near the cylinder entrance because the fluid is cold at the inlet and then, it rises along the cylinder due to the heat transfer, which increases the fluid flow temperature. It can be concluded that far away from the entrance, the effect of slip condition would be insignificant.

Figure 10 shows the dimensionless temperature pattern along the vertical line at $x = L$ for water-CMC/TiO_2 nano-fluid with $\varphi = 0.04$ at $Re = 10$ under different slip conditions. As shown, the dimensionless temperature at the center of the cylinder increases by increasing the slip coefficient. According to Figure 9, followed by applying the slip condition, the temperature of the fluid which is located in the vicinity of the walls decreases; therefore, the temperature distinct for the wall and the fluid become larger, hence greater heat exchanging between the solid wall and fluid and higher fluid temperature and dimensionless temperature, as well.

Figure 11 presents the local Nusselt number along the inner and outer walls for different slip coefficients. This figure also shows the impact of slip condition on the Nusselt number for water/CMC-TiO_2 solution with the nano-particle volume fraction flow of 0.04 at a Reynolds number of 10. The local Nu number increased upon increasing the slip coefficient. As discussed earlier in Figure 10, given that the temperature on the vertical line of the flow with a large slip coefficient is higher, this flow experiences a higher bulk temperature on

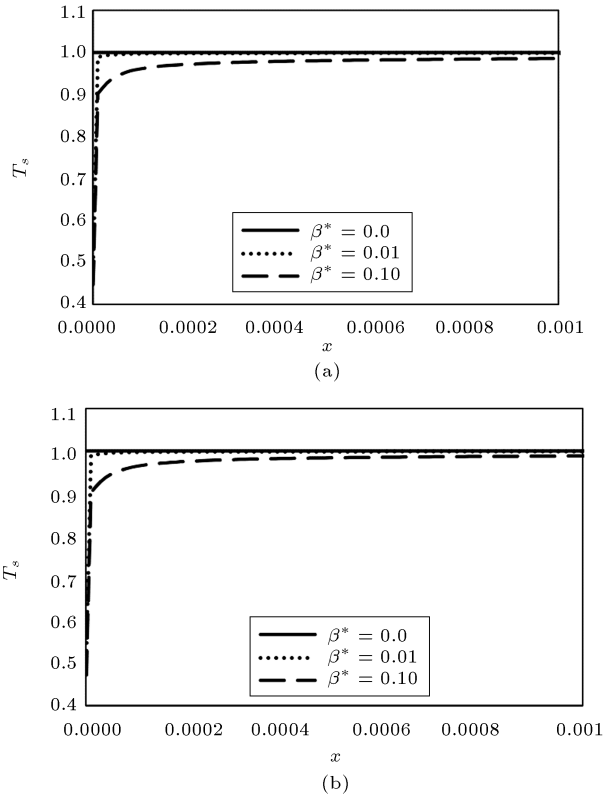

Figure 10. Temperature jump for non-Newtonian nano-fluid $\varphi = 0.04$ at $Re = 10$ and various slip coefficients along (a) inner wall and (b) outer wall.

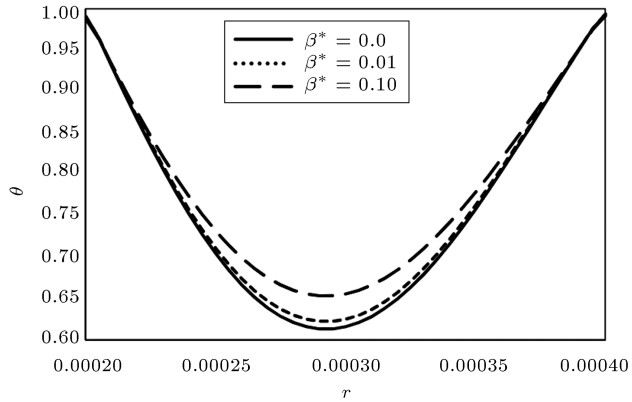

Figure 11. Dimensionless temperature profile for non-Newtonian nano-fluid at the exit of cylinder for different slip coefficients, $Re = 10$, and $\varphi = 0.04$.

each cross-section than that of no-slip flow. According to the definition of the Nusselt number, it has an inverse relationship with temperature difference; in other words, the Nusselt number is large when the bulk temperature has a high value.

Figure 12 shows the local Nu near the walls of the annular cylinder for water-CMC/TiO_2 with the volume fraction of 0.04 at Reynolds number 10, considering the slip wall and temperature jump ($\beta = 0.1$). Clearly, the local Nu of the inner wall is higher than that

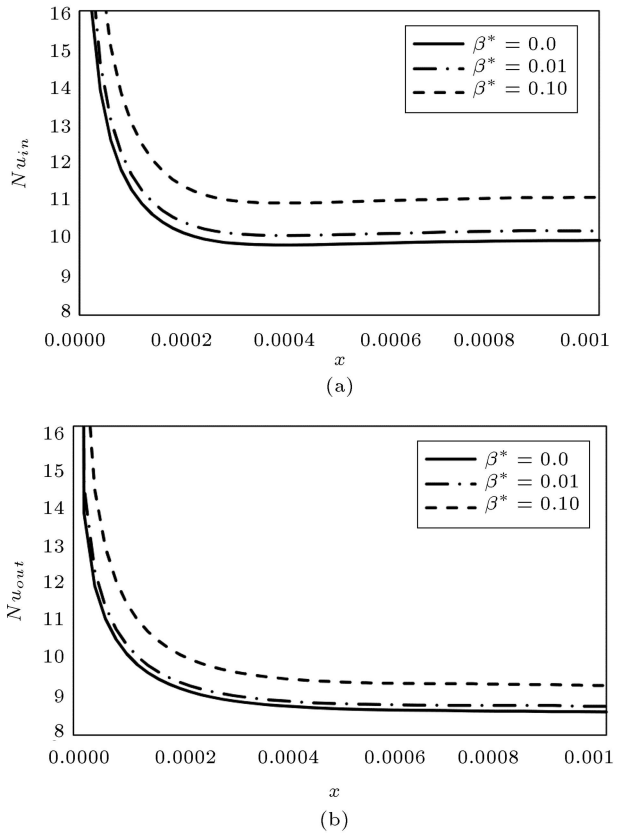

Figure 12. Local Nusselt number for non-Newtonian nano-fluid for different slip coefficients, $Re = 10$, and $\varphi = 0.04$ along (a) inner wall and (b) outer wall.

of the outer one mainly due to the non-Newtonian performance of the fluid.

Figure 13 illustrates the shear ratio of water-CMC/TiO_2 with a volume fraction of 0.04 at a Reynolds number of 10 along the vertical line at $x = 0.00025$. In this figure, the shear rate in the vicinity of the inner wall is higher than that near the outer walls. According to the shear-thinning fluid behavior, when the flow has a higher shear rate, the apparent viscosity is low. Accordingly, it can be concluded that

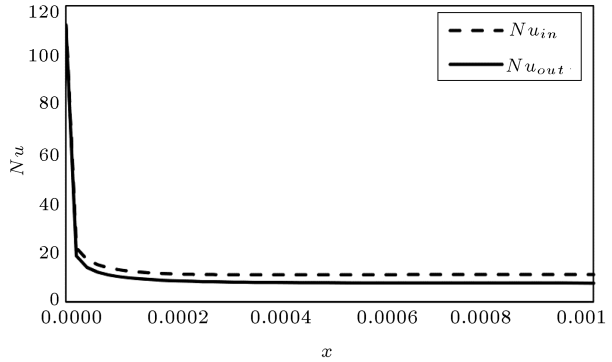

Figure 13. Local Nusselt number for non-Newtonian nano-fluid along inner and outer walls with $\varphi = 0.04$ at $Re = 10$ and $\beta = 0.1$.

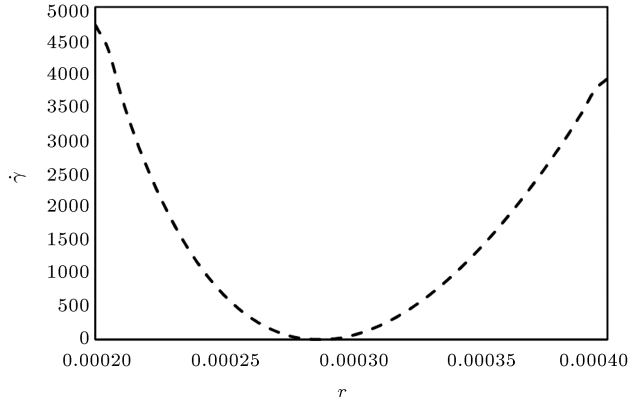

Figure 14. Shear rate for non-Newtonian nano-fluid along radial line $x = 0.00025$, with $\varphi = 0.04$ at $Re = 10$ and $\beta = 0.1$.

the apparent viscosity of the flow close to the inner wall is low, which reduces the impact of viscosity force and improves the heat transfer due to the convection-advection phenomenon.

Figure 14 lists the local Nusselt numbers at different Reynolds numbers along the inner and outer walls of the annular cylinder for $\varphi = 0.04$ and $\beta = 0.1$. It also indicates that as expected for both walls, the local Nusselt number increases upon increasing the Reynolds number mainly because of the non-Newtonian performance of the fluid. In addition, the enhancement of the Nusselt number is affected by a gradual increase in the RN, which is much higher at lower ones. Further, the Nu on the inner wall is higher than that on the outer wall mainly because the temperature of the outer wall is higher than that of the inner one.

As shown in Figure 15, the apparent viscosity decreases by increasing Re. At small Reynolds number (i.e., $Re = 1$) which results in low viscosity, the heat transfer mostly occurs as conduction. On the contrary, for higher Reynolds numbers, the viscosity force imposed on the fluid is smaller due to the decreasing viscosity, and heat can be transferred as a convection part in addition to the conduction part. In the power-law approach, the viscosity relates to the velocity gradient, power law (n), and consistency (m). In the wall nearby, the viscosity at a larger Reynolds number is less than that in the low laminar flows, probably because decreasing the Reynolds number would cause a decrease in the velocity gradient. The change pattern considering the distance from the wall shows that the viscosity at $r = 0.0003$ is greater than $r = 0.0002$ due to the slow development of the hydrodynamic boundary layer at larger Reynolds numbers, being in agreement with the findings obtained in [21]. Consequently, the velocity gradients get larger in central areas and greater viscosity can be expected in the center parts at $Re = 1$ by the velocity gradient at lower values.

Figure 16 shows the local Nu for non-Newtonian

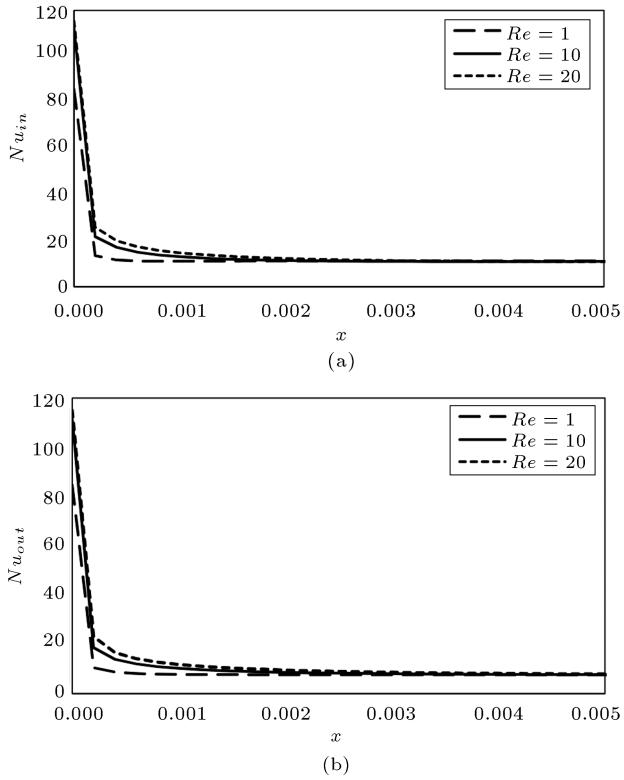

Figure 15. Local Nusselt number for non-Newtonian nano-fluid at various Reynolds numbers, $\beta = 0.1$ and $\varphi = 0.04$, along (a) inner wall and (b) outer wall.

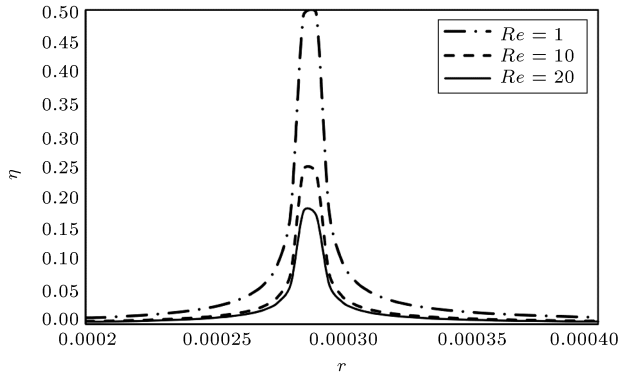

Figure 16. Apparent viscosity for non-Newtonian nano-fluid on the radial line $x = 0.00025$ at different Re, $\beta = 0.1$, and $\varphi = 0.04$.

nano-fluid at different volume fractions along the inner and outer walls of an annular cylinder at $Re = 10$ and $\beta = 0.1$. For both walls, the nano-fluid with a high fraction volume has a larger local Nusselt number because the thermal conductivity of nano-particles is more significant than that of the pure fluid and the addition of nano-particles would increase the effective thermal conductivity. As a result, the local Nusselt number increases upon increasing the volume fraction of nano-particles.

As illustrated in Figure 17, the apparent viscosity of the fluid increases by adding nano-particles. As mentioned earlier, it has a negative impact on the heat transfer rate regarding the imposed higher viscosity force on the fluid. However, the positive impact outweighs the negative one and the addition of nano-particles may enhance the rate of heat transfer. According to the findings, following an increase in the volume fraction of the nanoparticles to values higher than 0.04% by volume, the strain of nanofluid layers loses its linearity with respect to other shear stresses and becomes nonlinear, implying that the nature of the fluid changes from Newton to non-Newtonian fluid.

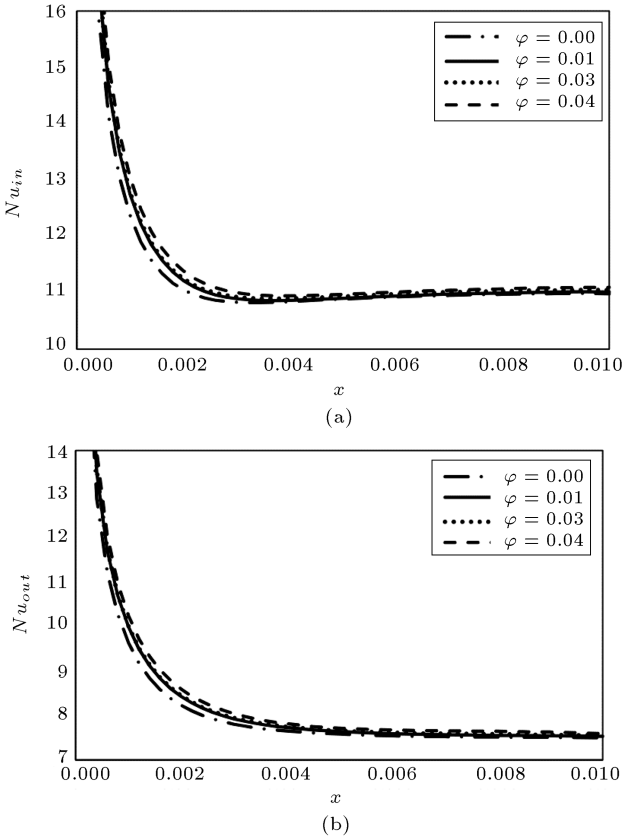

Figure 17. Local Nusselt number for non-Newtonian nano-fluid with different volume fractions, $Re = 10$, and $\beta = 0.1$ along (a) inner wall and (b) outer wall.

5. Conclusion

Nanofluids, obtained from the distribution of nanoscale particles in ordinary fluids, represent a novel generation of fluids with great potential in various applications. The effect of different physical parameters governing the problem, such as magnetic, slip velocity, and suction parameters, on the velocity and temperature curves such as Entropy Generation (EG) was also evaluated. The velocity is highly related to the sliding velocity parameter, and with an increase in the sliding velocity parameter, the velocity is reduced. The current study numerically investigated the first and second

laws of non-Newtonian nano-fluid flow through micro-annulus in terms of slip velocity and temperature jump. The flow was assumed to be laminar, steady-state, incompressible, axisymmetric, and single-phase. The properties of water-CMC/TiO_2 solution were considered in the simulation of the working fluid. In addition, the impacts of Re, volume fraction of nano-particles, slip velocity, and temperature jump on EG, Nusselt number, and Bejan numbers were evaluated and the findings were discussed considering the non-Newtonian behavior of the working fluid. The concluding remarks are summarized below:

- The EG rate was very high at the input parts and it decreased over the annular tube. Therefore, it can be concluded that EG is more significant in the undeveloped part of flows;
- For the walls nearby, the local Nusselt number increased upon increasing the slip velocity;
- Nusselt number in the interior wall was higher than that at the outer walls mainly because the shear rate in the vicinity of the interior wall was higher than that at outside walls;
- Given the shear-thinning fluid behavior, when the flow has a higher shear rate, the apparent viscosity is small. Therefore, the apparent viscosity of the flow close to the inner wall was low, which in turn attenuated the impact of the viscosity force and improved the heat transfer due to the convection-advection phenomenon.

Nomenclature

x	Axial direction
r	Radial direction
L	Length of geometry
r_i	Inner radius
r_o	Outer radius
$\vec{U}$	Velocity vector
T	Temperature
P	Pressure
$\bar{\bar{\tau}}$	Shear rate tensor
ρ_{nf}	Density of nano-fluid
$C_{p_{nf}}$	Specific heat of nano-fluid
k_{nf}	Thermal conductivity of nano-fluid
ν	Apparent viscosity
$\dot{\bar{\gamma}}$	Shear rate tensor
$\dot{\gamma}$	Shear ratio
m	Consistency index
n	Power-law
U	Dimensionless velocity
U_m	Mean velocity
u_s	Slip velocity
D	Hydraulic diameter
h	Heat transfer coefficient
Re	Reynolds number
Nu	Nusselt number
T_b	Bulk temperature
T_s	Surface temperature (temperature jump)
T_w	Wall temperature
θ	Dimensionless temperature
q''	Wall heat flux
S_t	EG rate
S_h	EG rate regarding heat transfer
S_f	EG rate regarding viscous effect
Be	Bejan number
φ	Nano-particle volume fraction
F_t	Thermal adaptation coefficient
F_m	Adaptation coefficient
β	Slip velocity coefficient
Pr	Prandtl number

References

1. Bejan, A. "Second-law analysis in heat transfer and thermal design", In *Advances in Heat Transfer*, **8**, pp. 1–58 (1982).
2. Chupradit, S., Jalil, A.T., Enina, Y., et al., *Use of Organic and Copper-Based Nanoparticles on the Turbulator Installment in a Shell Tube Heat Exchanger: A CFD-Based Simulation Approach by Using Nanofluids*, Journal of Nanomaterials (2021).
3. Hashemi, M.M., Nikfarjam, A., and Raji, H. "Novel fabrication of extremely high aspect ratio and straight nanogap and array nanogap electrodes", *Microsystem Technologies*, **25**(2), pp. 541–549 (2019).
4. Nabavi, M., Nazarpour, V., Alibak, A.H., et al. "Smart tracking of the influence of alumina nanoparticles on the thermal coefficient of nanosuspensions: application of LS-SVM methodology", *Applied Nanoscience*, **11**(7), pp. 2113–2128 (2021).
5. Hoseini, M., Haghtalab, A., and Navid Family, M. "Elongational behavior of silica nanoparticle-filled low-density polyethylene/polylactic acid blends and their morphology", *Rheologica Acta*, **59**, pp. 621–630 (2020). https://doi.org/10.1007/s00397-020-01225-5
6. Tjahjono, T., Elveny, M., Chupradit, S., et al. "Role of cryogenic cycling rejuvenation on flow behavior of Zr-CuAlNiAg metallic glass at relaxation temperature", *Transactions of the Indian Institute of Metals*, **74**, pp. 3241–3247 (2021). https://doi.org/10.1007/s12666-021-02395-3

7. Al-Shawi, S.G., Andreevna Alekhina, N., Aravindhan, S., et al. "Synthesis of NiO nanoparticles and sulfur, and nitrogen co doped-graphene quantum dots/nio nanocomposites for antibacterial application", *Journal of Nanostructures*, **11**(1), pp. 181–188 (2021).

8. Norouzi, M. and Rezaie, M.R. "An exact analysis on heat convection of nonlinear viscoelastic flows in isothermal microtubes under slip boundary condition", *Journal of the Brazilian Society of Mechanical Sciences and Engineering*, **40**(9), pp. 1–7 (2018).

9. Chen, H., Bokov, D., Chupradit, S., et al. "Combustion process of nanofluids consisting of oxygen molecules and aluminum nanoparticles in a copper nanochannel using molecular dynamics simulation", *Case Studies in Thermal Engineering*, **28**(3), p. 101628 (2021).

10. Sani, M.H., Sami, P., Shen, C., et al. "High resolution biosensor with simultaneous detection of two refractive index sample in optical microstructure", *Journal of Research in Science, Engineering and Technology*, **9**(03), pp. 64–75 (2021).

11. Watandost, H., Achak, J., and Haqmal, A. "Oxidation of hydrogels based of sodium alginate and MnO_2 as catalyst", *International Journal of Innovative Research and Scientific Studies*, **4**(4), pp. 191–199 (2021). https://doi.org/10.53894/ijirss.v4i4.77

12. Pham, Q.H., Chupradit, S., Widjaja, G., et al. "The effects of Ni or Nb additions on the relaxation behavior of Zr55Cu35Al10 metallic glass", *Materials Today Communications*, **29**(1), p. 102909 (2021).

13. Jahanmahin, O., Kirby, D.J., Smith, B.D., et al. "Assembly of gold nanowires on gold nanostripe arrays: simulation and experiment", *The Journal of Physical Chemistry C.*, **124**(17), pp. 9559–9571 (2020).

14. Mojtabavi, L. and Razavi, A. "The effects of addition of copper on the structure and antibacterial properties of biomedical glasses", *European Chemical Bulletin*, **9**(1), pp. 1–5 (2020).

15. Abdulrazzaq, T., Togun, H., Goodarzi, M., et al. "Turbulent heat transfer and nanofluid flow in an annular cylinder with sudden reduction", *Journal of Thermal Analysis and Calorimetry*, **141**(1), pp. 373–385 (2020).

16. Tayebi, T., Öztop, H.F., and Chamkha, A.J., "MHD natural convection of a CNT-based nanofluid-filled annular circular enclosure with inner heat-generating solid cylinder", *The European Physical Journal Plus*, **136**(2), pp. 1–21 (2021).

17. He, W., Toghraie, D., Lotfipour, A., et al. "Effect of twisted-tape inserts and nanofluid on flow field and heat transfer characteristics in a tube", *International Communications in Heat and Mass Transfer*, **110**, pp. 34–56 (2020).

18. Chen, Y., Shen, C., Shi, M., et al. "Visualization study of flow condensation in hydrophobic microchannels", *AIChE Journal*, **60**(3), pp. 1182–1192 (2014).

19. Fu, C., Rahmani, A., Suksatan, W., et al. "Comprehensive investigations of mixed convection of Fe-ethylene-glycol nanofluid inside an enclosure with different obstacles using lattice Boltzmann method", *Scientific Reports*, **11**(1), pp. 1–16 (2021).

20. Shan, B., Wang, P., Zhang, Y., et al. "Discrete unified gas kinetic scheme for all Knudsen number flows. IV. Strongly inhomogeneous fluids", *Physical Review E.*, **101**(4), pp. 34–56 (2020).

21. Pathare, P.G., Tekale, S.U., Damale, M.G., et al. "Pyridine and benzoisothiazole based pyrazolines: synthesis, characterization, biological activity, molecular docking and ADMET study", *European Chemical Bulletin*, **9**(1), pp. 10–21 (2020).

22. Reddy, N.A., Kamala, K., Dayam, R., et al. "Glycerol mediated one-pot synthesis of pyrazole conjugated tetrahydroquinoline derivatives and evaluation of their anticancer activity", *European Chemical Bulletin*, **9**(9), pp. 300–305 (2020).

23. Talavari, A., Ghanavati, B., Azimi, A., et al. "PVDF/MWCNT hollow fiber mixed matrix membranes for gas absorption by Al_2O_3", *Nanofluid Progress in Chemical and Biochemical Research*, **4**(2), pp. 177–190 (2021). DOI: 10.22034/pcbr.2021.270178.1177

24. Adebayo, M.A., Akande, S.O., Olorunfemi, A.D., et al. "Equilibrium and thermodynamic characteristics of the corrosion inhibition of mild steel using sweet prayer leaf extract in alkaline medium", *Progress in Chemical and Biochemical Research*, **4**(1), pp. 80–91 (2021). DOI: 10.22034/pcbr.2021.120449

25. Malvandi, A. and Ganji, D. "Brownian motion and thermophoresis effects on slip flow of alumina/water nanofluid inside a circular microchannel in the presence of a magnetic field", *International Journal of Thermal Sciences*, **84**, pp. 196–206 (2014).

26. Zhang, T., Jia, L., Yang, L., et al. "Effect of viscous heating on heat transfer performance in microchannel slip flow region", *International Journal of Heat and Mass Transfer*, **53**(21–22), pp. 4927–4934 (2010).

27. Shamshiri, M., Ashrafizaadeh, M., and Shirani, E., "Effects of rarefaction, viscous dissipation and rotation mode on the first and second law analyses of rarefied gaseous slip flows confined between a rotating shaft and its concentric housing", *Energy*, **37**(1), pp. 359–370 (2012).

28. Yari, M. "Second-law analysis of flow and heat transfer inside a microannulus", *International Communications in Heat and Mass Transfer*, **36**(1), pp. 78–87 (2009).

29. Zhao, J. "Axisymmetric convection flow of fractional Maxwell fluid past a vertical cylinder with velocity slip and temperature jump", *Chinese Journal of Physics*, **67**, pp. 501–511 (2020).

30. Erbay, L.B., Yalçın, M.M., and Ercan, M.Ş., "EG in parallel plate microchannels", *Heat and Mass Transfer*, **43**(8), pp. 729–739 (2007).

31. Karimipour, A., Ghasemi, S., Darvanjooghi, M.H.K., et al. "A new correlation for estimating the thermal conductivity and dynamic viscosity of CuO/liquid paraffin nanofluid using neural network method", *International Communications in Heat and Mass Transfer*, **92**, pp. 90–99 (2018).

32. Jangili, S., Gajjela, N., and Beg, O.A. "Mathematical modeling of EG in magnetized micropolar flow between co-rotating cylinders with internal heat generation". *Alexandria Engineering Journal*, **55**(3), pp. 1969–1982 (2016).

33. Thumma, T., Mishra, S., and Bég, O.A. "ADM solution for Cu/CuO-water viscoplastic nanofluid transient slip flow from a porous stretching sheet with EG, convective wall temperature and radiative effects", *Journal of Applied and Computational Mechanics*, **78**, pp. 1–15 (2021).

34. Galchynska, J., Larina, Y., Varchenko, O., et al., "Perspectives of Ukrainian bioenergy development estimation by means of cluster analysis and marketing approach", *Economic Annals-I*, **187**(1–2), pp. 63–74 (2021).

35. Al-warda, H.S., Ahmed, M.R., and Al-Abachi, M.Q. "Thermodynamic study and spectrophotometric determination of cefixime trihydrate in pure form and pharmaceutical tablets using batch and normal flow injection analysis", *Eurasian Chemical Communications*, **3**(7), pp. 495–507 (2021). DOI: 10.22034/ecc.2021.289383.1183

36. Abdulrazzaq, T., Togun, H., Goodarzi, M., et al. "Turbulent heat transfer and nanofluid flow in an annular cylinder with sudden reduction", *Journal of Thermal Analysis and Calorimetry*, **141**(1), pp. 373–85 (2018).

37. Sarafraz, M.M., Shadloo, M.S., Tian, Z., et al. "Convective bubbly flow of water in an annular pipe: role of total dissolved solids on heat transfer characteristics and bubble formation", *Water*, **11**(8), p. 1566 (2018).

38. Anand, V. "Slip law effects on heat transfer and EG of pressure driven flow of a power law fluid in a microchannel under uniform heat flux boundary condition", *Energy*, **76**, pp. 716–732 (2014).

39. Kiyasatfar, M. "Convective heat transfer and EG analysis of non-Newtonian power-law fluid flows in parallel-plate and circular microchannels under slip boundary conditions", *International Journal of Thermal Sciences*, **128**, pp. 15–27 (2018).

40. Ramanuja, M., Krishna, G.G., Sree, H.K., et al. "Free convection in a vertical slit micro-channel with superhydrophobic slip and temperature jump conditions", *Journal Homepage*, **38**(3), pp. 738–744 (2020).

41. Li, Y., Kalbasi, R., Karimipour, A., et al. "Using of Artificial Neural Networks (ANNs) to predict the rheological behavior of MgO-Water nanofluid in a different volume fraction of nanoparticles, temperatures, and shear rates", *Authorea Preprints*, **56**(4), pp. 78–97 (2020).

42. Lin, Y., Zheng, L., and Zhang, X. "Radiation effects on marangoni convection flow and heat transfer in pseudo-plastic non-Newtonian nanofluids with variable thermal conductivity", *International Journal of Heat and Mass Transfer*, **77**, pp. 708–716 (2014).

43. Ghalandari, M., Mirzadeh Koohshahi, E., Mohamadian F., et al. "Numerical simulation of nanofluid flow inside a root canal", *Engineering Applications of Computational Fluid Mechanics*, **13**(1), pp. 254–264 (2019).

44. Campbell, C.S. and Gong, A. "The stress tensor in a two-dimensional granular shear flow", *Journal of Fluid Mechanics*, **164**, pp. 107–125 (1986).

45. Gabbanelli, S., Drazer, G., and Koplik, J. "Lattice Boltzmann method for non-Newtonian (power-law) fluids", *Physical Review E.*, **72**(4), pp. 45–67 (2005).

46. Hojjat, M., Etemad, S.G., Bagheri, R., et al. "Rheological characteristics of non-Newtonian nanofluids: experimental investigation", *International Communications in Heat and Mass Transfer*, **38**(2), pp. 144–148 (2011).

47. Ahmadizadeh, P., Mashadi, B., and Lodaya, D. "Energy management of a dual-mode power-split powertrain based on the Pontryagin's minimum principle", *IET Intelligent Transport Systems*, **11**(9), pp. 561–571 (2017).

48. Satapathy, A.K. "Slip flow heat transfer in an infinite microtube with axial conduction", *International Journal of Thermal Sciences*, **49**(1), pp. 153–160 (2010).

49. Al-Kahtani, A.A., Tabassum, S., Raya, I., et al. "Influence of different rotations of organic formamidinium molecule on electronic and optical properties of FAPbBr3 Perovskite", *Coatings*, **11**(11), p. 1341 (2021).

50. Bahiraei, M. and Alighardashi, M. "Investigating non-Newtonian nanofluid flow in a narrow annulus based on second law of thermodynamics", *Journal of Molecular Liquids*, **219**, pp. 117–127 (2016).

51. Anggono, A.D., Elveny, M., Abdelbasset, W.K., et al. "Creep deformation of Zr55Co25Al15Ni5 bulk metallic glass near glass transition temperature: A nanoindentation study", *Transactions of the Indian Institute of Metals*, **75**(3), pp. 673–680 (2021).

Biographies

Farshid Mehran received his BSc in Mechanical Engineering while working in various areas of this major, including Fluid Mechanics and Thermodynamics. He later completed his MSc in Mechanical Engineering from Islamic Azad University. His research interests

are non-newton fluids, micro fluids, and computational fluid dynamics.

Ali Jabbarzadeh Ghandilou is an MSc in Mechanical Engineering graduated from University of Tabriz. He is a Researcher in the Engine and Thermal Systems at the Department of Mechanical Engineering, and his current research interests focused on the computational fluid dynamics, fluid flow, and heat transfer.

Lis M. Yapanto is a Researcher at the Universitas Negeri Gorontalo. Her research interests are the energy and environmental issues with emphasis on the oil industry. She has published numerous peer-reviewed articles in the fields of mathematical modeling, energy, and fluid flow.